Pulse-width modulated external resistance increases the microbial fuel cell power output

Coronado, J.; Perrier, M.; Tartakovsky, B.

Publisher's version / Version de l'éditeur:
https://doi.org/10.1016/j.biortech.2013.08.005
Bioresource Technology, 147, pp. 65-70, 2015-08-09

AUTHOR QUERY FORM

ELSEVIER	**Journal: BITE** **Article Number: 12203**	**Please e-mail or fax your responses and any corrections to:** **E-mail: corrections.esch@elsevier.sps.co.in** **Fax: +31 2048 52799**

Dear Author,

Please check your proof carefully and mark all corrections at the appropriate place in the proof (e.g., by using on-screen annotation in the PDF file) or compile them in a separate list. Note: if you opt to annotate the file with software other than Adobe Reader then please also highlight the appropriate place in the PDF file. To ensure fast publication of your paper please return your corrections within 48 hours.

For correction or revision of any artwork, please consult http://www.elsevier.com/artworkinstructions.

Any queries or remarks that have arisen during the processing of your manuscript are listed below and highlighted by flags in the proof. Click on the 'Q' link to go to the location in the proof.

Location in article	**Query / Remark: click on the Q link to go** **Please insert your reply or correction at the corresponding line in the proof**
Q1	Please confirm that given name(s) and surname(s) have been identified correctly.
	Please check this box if you have no corrections to make to the PDF file ☐

Thank you for your assistance.

Bioresource Technology xxx (2013) xxx–xxx

Contents lists available at ScienceDirect

Bioresource Technology

journal homepage: www.elsevier.com/locate/biortech

Pulse-width modulated external resistance increases the microbial fuel cell power output

J. Coronado [a], M. Perrier [a], B. Tartakovsky [b,*]

[a] Departement de Génie Chimique, École Polytechnique Montréal, C.P.6079 Succ., Centre-Ville Montréal, QC H3C 3A7, Canada
[b] National Research Council of Canada, 6100 Royalmount Ave., Montréal, QC H4P 2R2, Canada

HIGHLIGHTS

- MFC is operated with pulse-width modulated connection of the electrical load.
- At operating frequencies above 100 Hz power output increases by 22–43%.
- Process dynamics can be described by a simple equivalent circuit model.

ARTICLE INFO

Article history:
Received 30 April 2013
Received in revised form 31 July 2013
Accepted 2 August 2013
Available online xxxx

Keywords:
MFC
Periodic operation
Pulse-width modulation
Power output maximization

ABSTRACT

This study describes MFC operation with a pulse-width modulated connection of the external resistor (R-PWM mode) at low and high frequencies. Analysis of the output voltage profiles acquired during R-PWM tests showed the presence of slow and fast dynamic components, which can be described by a simple equivalent circuit model suitable for process control applications. At operating frequencies above 100 Hz a noticeable improvement in MFC performance was observed with the power output increase of 22–43% as compared to MFC operation with a constant external resistance.

1. Introduction

Environmental and economic sustainability requires a number of changes in the existing energy production and consumption practices. Not only would fossil fuels be replaced with renewable sources of energy, but also our energy consumption should be reduced by using energy-efficient technologies. With this regard, electricity production from organic wastes in Microbial Fuel Cells (MFCs) offers a new technological solution capable of converting otherwise energy-consuming wastewater treatment into an energy-neutral, and potentially an energy-producing process.

Advances in MFC design and materials helped to improve volumetric power output by several orders of magnitude (Logan, 2010). Yet, to be competitive with the existing wastewater treatment technologies, power densities should be further improved. While researchers continue to make progress by improving the electrode materials and MFC design (Logan, 2010; Saito et al., 2011; Song et al., 2010), the need for an adequate electrical system for optimized energy collection also becomes more and more apparent (Premier et al., 2011; Woodward et al., 2010; Woodward et al., 2009).

In order to utilize MFCs for powering electrical devices, a relatively low output voltage, which typically ranges from 0.2 to 0.5 V, should be converted to a higher value using an electronic device (boost converter or up-converter). Recently, several power management systems for up-converting MFC output voltage have been suggested (Park and Ren, 2012a; Tender et al., 2008; Wu et al., 2012; Yang et al., 2012), including a synchronous boost converter (Park and Ren, 2012a), a transformer – based power management system (Yang et al., 2012), and a custom-made power conditioner, which transformed the voltage from 0.35 to 6 V (Tender et al., 2008).

In addition to voltage conversion, MFC power output might be maximized by matching the external impedance with MFC internal impedance. Based on the principle of power supply by means of commuting (switching) circuits, hysteresis controllers have been implemented to track the Maximum power point (MPP) of a MFC (Park and Ren, 2012b). Also, a perturbation-observation algorithm was used to optimize MFC electrical load in real time showing a considerably improved power output (Pinto et al., 2011b; Woodward et al., 2010). In addition, a simple heuristic approach was

* Corresponding author. Tel.: +1 514 496 2664; fax: +1 514 496 6265.
E-mail address: Boris.Tartakovsky@cnrc-nrc.gc.ca (B. Tartakovsky).

0960-8524/$ - see front matter © 2013 Published by Elsevier Ltd.
http://dx.doi.org/10.1016/j.biortech.2013.08.005

implemented to automatically control the electrical load attached to the MFC (Premier et al., 2011).

At least one recent study suggested that by operating an MFC with intermittent connection/disconnection of the electrical load (external resistance), the MFC power output could be improved (Grondin et al., 2012). The study presented below elaborates on the approach of intermittent (periodic) connection of the electrical load by analyzing the MFC frequency response in a range of 0.1–1000 Hz and operating the MFC at a sufficiently high switching frequency, equivalent to a pulse-width modulated connection of the external resistance (R-PWM mode of operation).

2. Methods

2.1. MFC design, inoculation, and operation

Two membrane-less air-cathode MFCs were constructed using nylon plates as described elsewhere (Grondin et al., 2012). The anodes were 5 mm thick carbon felts measuring 10 cm × 5 cm (SGL Canada, Kitchener, ON, Canada) and the cathodes were 10 cm × 5 cm manganese-based catalyzed carbon E4 air cathodes (Electric Fuel Ltd, Bet Shemesh, Israel). The electrodes were separated by a nylon cloth. Two MFCs, MFC-1 and MFC-2, were built. Both MFCs had an anodic compartment volume of 50 mL. MFC-1 contained two 10 cm × 5 cm carbon felt anodes with a total thickness of 10 mm and two cathodes (one on each side connected by a wire) with a total surface area of 100 cm^2. MFC-2 had one 10 cm × 5 cm carbon felt anode with a thickness of 5 mm and one 50 cm^2 cathode.

Each MFC was inoculated with 5 mL of anaerobic sludge with volatile suspended solids (VSS) content of approximately 40–50 g L^{-1} (Lassonde Inc., Rougemont, QC, Canada) and 20 mL of effluent from an operating MFC. The MFCs were maintained at 25 °C and were continuously fed with sodium acetate and trace metal solutions using a syringe pump and a peristaltic pump, respectively. The acetate stock solution was composed of (in g L^{-1}): sodium acetate (37.0), yeast extract (0.8), NH_4Cl (18.7), KCl (148.1), K_2HPO_4 (64.0), and KH_2PO_4 (40.7). The infusion rate of the acetate stock solution was varied in order to obtain the desired influent concentration. The trace metal solution was prepared by adding 1 mL of the trace elements stock solution to 1 L of deionized water. A detailed composition of the stock solution of the trace elements is given elsewhere (Pinto et al., 2011a).

An influent acetate concentration of 900 mg L^{-1} and a hydraulic retention time of 6–7 h were typically maintained, with an exception of the high-load test, where the influent acetate concentration was doubled to 1800 mg L^{-1}. Fig. 1A shows the schematic diagram of the experimental setup, while a detailed description of MFC design, stock solution composition, and operating conditions can be found elsewhere (Grondin et al., 2012).

2.2. External resistance connection

Pulse-width modulated connection of the external resistor (R_{ext}) to MFC terminals was achieved by adding an electronic switch (IRF540, International Rectifier, El Sequndo, CA, USA) to the external electrical circuit (denoted as SW in Fig. 1B, the corresponding resistance is shown as R_{SW}). Duty cycle (D) was defined as:

$$D = \frac{t_{on}}{t_{off} + t_{on}} 100\% \quad (1)$$

Where t_{on} is the "on" time within each cycle during which R_{ext} is connected and t_{off} is the disconnection ("off") time. The electronic switch was computer-controlled using a Labjack U3-LV data

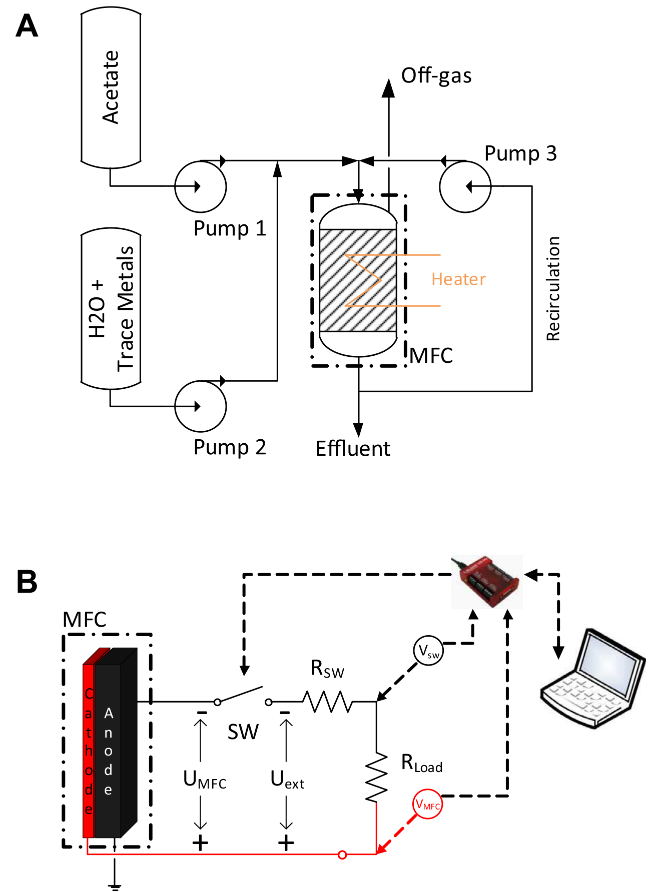

Fig. 1. Schematic diagrams of the experimental setup (A) and electrical circuit (B).

acquisition board (LabJack Corp., Lakewood, CO, USA). The data acquisition board was also used to record MFC voltage at a maximum rate of 22,500 scans/s.

As shown in Fig. 1B, the data acquisition board measured MFC output voltage (U_{MFC}) and voltage after the switch (U_{sw}). Electrical connections corresponding to these measurements are shown in Fig. 1B as V_{MFC} and V_{SW}, respectively. Voltage over the resistive load (U_{Load}) was calculated as the difference between U_{MFC} and U_{sw} ($U_{Load} = U_{MFC} - U_{sw}$). Electric current was calculated as $I = U_{Load}/R_{Load}$ by applying Ohm's law over the external load resistance (R_{Load}).

For calculation purposes, the switching device was considered as an ideal switch in series with a resistance R_{sw} to represent power losses in the switch. R_{sw} value was estimated by dividing the voltage over the switch by the current. In the following discussion, R_{ext} denotes the sum of the external load connected to the circuit and the switch resistance ($R_{ext} = R_{Load} + R_{sw}$) with a corresponding external voltage U_{ext}, as follows from the diagram shown in Fig. 1B. The voltage measurements described above and the calculation method accounted for power losses due to the fast switching.

2.3. Frequency and duty cycle tests

Frequency and duty cycle tests were carried out with either 15 min or 1 h intervals between parameter changes. The tests were performed in a broad range of frequencies from 0.1 to 1000 Hz. Duty cycle was set to 50% when frequency tests were carried out. For the duty cycle analysis, duty cycles were varied between 5% and 100% at a constant frequency of 500 Hz. Between the R-PWM tests, the MFCs were operated using the Perturbation/Observation algorithm described below.

MFC performance was expressed in terms of average (per cycle) output voltage, current, and power output. Average values per cycle were obtained as follows:

$$M = \frac{1}{T}\int_0^T m(t)dt \tag{2}$$

where $m(t)$ is either the voltage, current, or power measurements at each moment of time t, T is the cycle duration ($T = t_{on} + t_{off}$), and $\overline{M}$ is the corresponding average value. Integrals were numerically calculated. To reduce errors due to sampling noise at least 100 average (per cycle) values were acquired and then the mean values were calculated.

2.4. Perturbation/observation algorithm

The perturbation observation (P/O) algorithm for maximum power point tracking (MPPT) was used to optimize MFC performance during the tests with a fixed external resistor (control tests) and between frequency and duty cycle tests. At each iteration, the P/O algorithm modified R_{ext} (digital potentiometer) with a predetermined amplitude (ΔR) at each iteration. The direction of resistance change was selected by comparing the value of the power output with that at the previous resistance. Once the algorithm converges to a vicinity of the optimum resistance value, the R_{ext} will oscillate around this optimum with a maximum distance of ΔR. A computer-controlled digital potentiometer with a resistance variation range from 4 to 130 Ω and a step of 1.25 Ω was used (Innoray Inc, Montreal, QC, Canada). A detailed description of the P/O algorithm can be found in Woodward et al. (2010).

2.5. Numerical methods

Computer simulations were carried out using the equivalent circuit model and model solutions described in the Appendix. Parameter estimation was carried out using Fmincon function of Matlab R2010a (Mathworks, Natick, MA, USA). In the parameter estimation procedure the root mean square error (RMSE) between the model outputs and measured values of U_{MFC} was minimized using data of five on/off cycles. At an R-PWM frequency of 0.1 Hz this corresponded to 637 data points. At a frequency of 100 Hz, 1000 data points were used to estimate model parameters.

3. Results and discussion

In order to evaluate the effect of a pulse-width modulated connection of the external resistance (R-PWM mode of operation), MFC-1 and MFC-2 were operated at several frequencies ranging from 0.1 Hz to 1000 Hz. At each tested frequency, R_{ext} was connected to the MFC during the first half of the cycle and disconnected for the rest of the cycle, thus corresponding to a duty cycle of 50%. Fig. 2A shows the average voltage output ($\overline{U}_{ext}$) calculated over the external resistor (R_{ext}) of MFC-1 during the R-PWM tests. The frequency tests were carried out with R_{ext} values of 8 and 47 Ω. It can be seen that in all tests the average voltage increased with the initial frequency increase, then a plateau was reached at around 100–500 Hz.

Initially, frequency tests were carried out with 15 min intervals between each frequency change. The tests were also repeated with 1 h intervals between the changes. A comparison of $\overline{U}_{ext}$ profiles obtained with 15 min and 1 h intervals shows a qualitatively similar dependence (Fig. 2A). However, the average voltage was always higher in the tests carried out with 1 h intervals, i.e., the average (per cycle) power output was improved. This suggests that

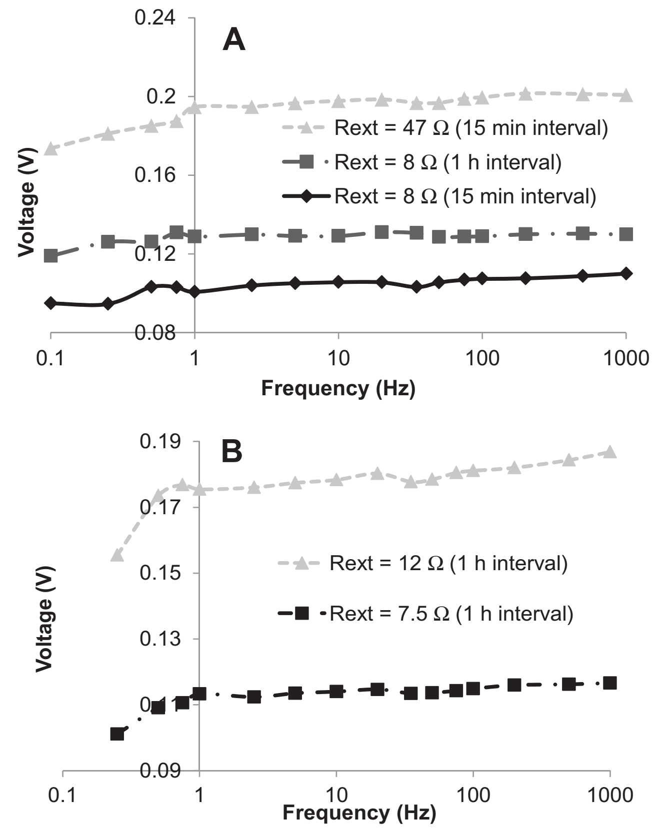

Fig. 2. Average external voltage $\overline{U}_{ext}$ as a function of R_{ext} connection - disconnection frequency.

a 15 min interval was insufficient to establish steady-state conditions corresponding to a new operating frequency. Also, it appeared that the R-PWM mode of operation led to an overall performance improvement, as power outputs were consistently higher as compared to a fixed R_{ext}. To insure reproducibility, the frequency tests were repeated in MFC-2 with R_{ext} values of 7.5 and 12 Ω. Once again, a similar trend was observed with a near linear increase of $\overline{U}_{ext}$ as the operating frequency increased from 0.1 Hz to 500 Hz (Fig. 2B). This increase in average voltage and, accordingly, in average power output was followed by $\overline{U}_{ext}$ stabilization at around 100–500 Hz.

MFC response to periodic connection/disconnection of R_{ext} was also characterized by observing the dynamics of MFC output voltage (U_{MFC}) during each cycle. Fig. 3 compares U_{MFC} values acquired during MFC-1 operation at a low frequency of 0.05 Hz (Fig. 3A, $D = 75\%$) and at a high frequency of 100 Hz (Fig. 3B, $D = 90\%$). It should be understood that when R_{ext} is connected, the output and external voltages are equal, i.e. $U_{MFC} = U_{ext}$. However, if R_{ext} is disconnected, then $U_{ext} = 0$, while $U_{MFC} > 0$. At both frequencies, MFC output voltage (U_{MFC}) abruptly decreases when R_{ext} is connected (closed circuit with switch ON), while it increases when R_{ext} is disconnected (open circuit with switch OFF). Also, when R_{ext} is connected to the MFC, current demand increases and a voltage divider is created between the MFC's internal impedance and the external resistance, causing U_{MFC} to decrease.

At 0.05 Hz two different dynamics components are evidenced during each on–off or off–on transition (Fig. 3A). At first, there is an abrupt change of U_{MFC} until reaching some intermediate value. This fast transition is followed by an exponential curve, which approaches the steady-state value at a much slower rate. At a frequency of 100 Hz (Fig. 3B), only fast dynamics appear in the U_{MFC} curve, while the slow dynamics disappears and U_{MFC} essentially

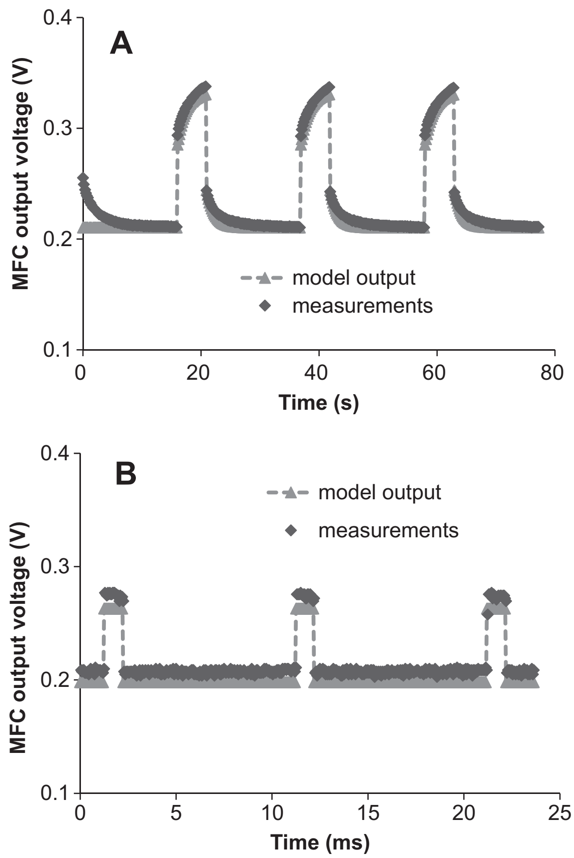

Fig. 3. Profiles of MFC voltage (U_{MFC}) measured at R_{ext} connection/disconnection frequencies of (A) 0.05 Hz (D = 75%)and (B) 100 Hz (D = 90%).

switches between two levels, with higher voltage corresponding to the open circuit state and lower voltage corresponding to the closed circuit state. This dynamics is consistent with the results of the frequency tests shown in Fig. 2 and can be described by a simple equivalent circuit model (Randles model, (Randles, 1947)) previously used for modeling batteries (Durr et al., 2006). The same equivalent circuit model was also recently used to simulate a MFC power management system (Yang et al., 2012). The model includes two resistors and a capacitor, which enables the description of the slow and fast output voltage responses observed during the tests. Fig. 4 shows the model diagram, where U_{oc} corresponds to MFC's open circuit voltage (ideal voltage), C represents the actual MFC capacitance, R_1 accounts for the MFC's ohmic losses, and R_2 represents the resistive component accounting for both the activation and concentration losses (Yang et al., 2012).

This equivalent circuit model might have a limited predictive capacity as it assumes that all the electrical elements are constant. Furthermore, this model does not consider any changes in biomass concentration, microbial activity, and carbon source concentration, i.e., constant values of these parameters are assumed. The MFC internal resistance and open circuit voltage were already demonstrated to be strongly dependent on biofilm density, on carbon source concentration in the anodic liquid, and on temperature (Pinto et al., 2010; (Pinto et al., 2011b). Therefore, the equivalent circuit model might be lacking the predictive capacity of bioelectrochemical models such as recently developed two-population bio-electrochemical MFC model (Pinto et al., 2010) and the conduction-based MFC model (Marcus et al., 2007) and cannot be used to predict the influence of various process inputs, such as the organic loading rate and the operating temperature, on MFC performance. Nevertheless, it offers some insight on the fast process dynamics linked to the electrical properties of a MFC. Indeed, when the electrical circuit is operated in the continuous mode (i.e., R_{ext} is constant), the internal capacitor is fully charged and the total internal resistance can be expressed as $R_{int} = R_1 + R_2$. The capacitor dynamics may only be evidenced when the system is disturbed, for example by means of a switch operated at a low frequency. Fig. 3 compares the equivalent circuit model outputs with voltage measurements at low (Fig. 3A) and high (Fig. 3B) frequencies of R_{ext} connection/disconnection. For this simulation, model parameters were estimated by minimizing RMSE between the measured voltage values and corresponding model outputs, as described above. The following parameters were estimated: $U_{oc} = 0.33$ V, $R_1 = 4.24\ \Omega$, $R_2 = 3.25\ \Omega$, $C = 0.38$ F. The comparison of simulated and measured voltage values shows that that the model adequately describes process dynamics at both frequencies, although at the high operating frequency the model appears to somewhat underestimate the output voltage. As mentioned above, although process dynamics is adequately described within each cycle, the model is too simplified to predict the output voltage over extended periods of time.

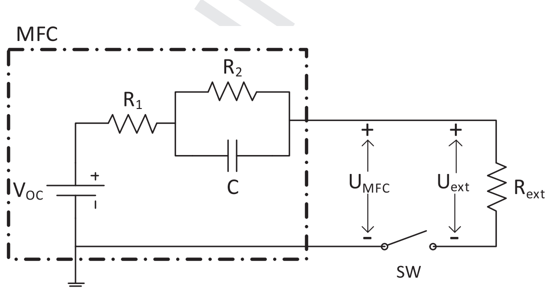

Fig. 4. MFC equivalent circuit model.

While the equivalent circuit model analysis might suggest that the power output is maximized at D equal to 100%, our previous study demonstrated improved MFC power output at D values below 100%, at least when the MFC was operated at very low frequencies below 0.1 Hz (Grondin et al., 2012). Consequently, the performance of MFC-1 and MFC-2 was evaluated in a series of tests (D tests) performed at a frequency of 500 Hz and various D values ranging from 5% to 100%, the latter corresponding to a fixed resistor.

Notably, MFC power output might also be dependent on the selected value of R_{ext}. Indeed, power output is maximized if external and internal impedances are matched. Therefore, prior to D tests total internal resistances (R_{int}) of MFC-1 and MFC-2 were estimated by conducting polarization tests and calculating R_{int} values using linear parts of each polarization curve. Based on this technique, both MFCs showed internal resistance values in a range of 12–15 Ω.

Fig. 5A shows MFC-1 power output at different values of the duty cycle and different external resistances. When D tests were conducted with $R_{ext} = 17\ \Omega$, which is slightly above the estimated value of R_{int} based on the corresponding polarization test, power output was maximized at $D = 95\%$. A duplicate test performed immediately after the first test demonstrated excellent reproducibility. Following this test, to compare R-PWM and mode of operation with the power output corresponding to a constant R_{ext}, MFC-1 was operated at $D = 100\%$ for three days. A slow decline in power output over time was observed with the power output stabilizing at 2.23 mW (Fig. 5A, $D = 100\%$). Interestingly, a re-evaluation of R_{int} suggested an increase to 20 Ω. A third D test conducted following MFC-1 operation with a constant R_{ext} confirmed a power output decrease (Fig. 5A).

D-tests were also performed in MFC-2 with $R_{ext} = 13.5\ \Omega$, which corresponded to an estimated value of R_{int}. In this test, MFC power

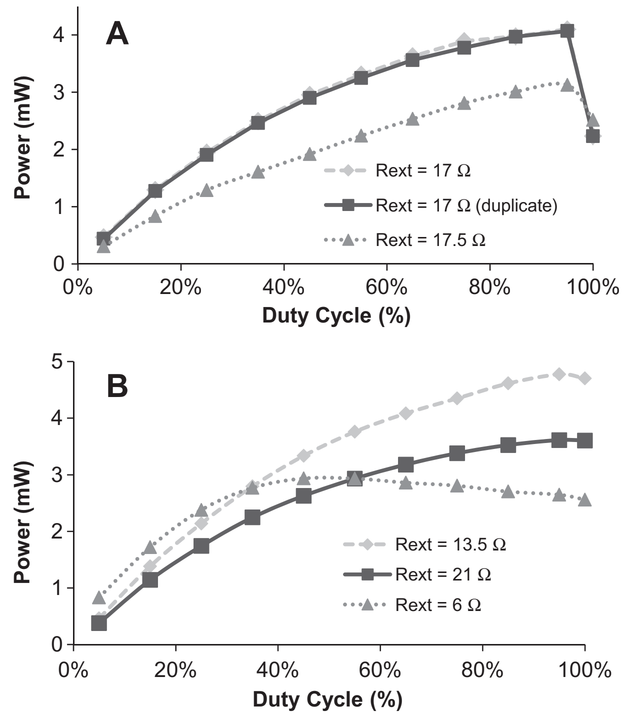

Fig. 5. MFC Power outputs of MFC-1 (A) and MFC-2 (B) as a function of their duty cycles. Power output at $D = 100\%$ corresponds to MFC operation with fixed external resistance. All D-tests were carried out at a frequency of 500 Hz.

Table 1
A comparison of average currents, power outputs an Coulombic Efficiencies (CE) obtained during R_{ext}-PWM and perturbation/observation tests carried out at two influent acetate concentrations.

Influent acetate(mg L^{-1})	Cell	R-PWM mode			Perturbation/observation		
		Current (mA)	Power (mW)	CE%	Current (mA)	Power (mW)	CE%
900	MFC-1	16.4	3.63	91.5	14.4	2.83	80.3
900	MFC-2	13.6	3.62	76.1	14.1	2.55	78.6
1800	MFC-1	15.1	3.84	42.2	17.1	3.07	47.9
1800	MFC-2	20.6	3.60	57.6	19.6	3.46	54.9

output at $D = 100\%$ was estimated using the same experimental procedure previously performed for other D values, i.e., the voltage was measured after 1 h of MFC-2 operation with a fixed resistor. Consequently, the power output decrease at $D = 100\%$ was much smaller as compared to $D = 95\%$ (Fig. 5B). When the test was repeated at $R_{ext} = 21\ \Omega$, which was above the estimated value of R_{int}, there was no difference between power outputs at $D = 95\%$ and $D = 100\%$. For the tests conducted at $R_{ext} = 6\ \Omega$ (well below R_{int} estimation), the power output was maximized at around $D = 45\%$, as can be seen from the data presented in Fig. 5B. Although this maximum was below the highest power output observed at R_{ext}–R_{int}, the R-PWM mode of operation prevented a sharp drop in power output typically observed at $R_{ext} \ll R_{int}$. and improved MFC stability by limiting the current. This feature might be especially useful to prevent voltage reversal in a stack of MFCs (Oh and Logan, 2007).

D-curves shown in Fig. 5 were in agreement with the results presented by Grondin et al.(2012), where the external load connection was governed by the upper and lower boundaries of the MFC output voltage, thus resulting in a variable switching frequency, which was below 0.1 Hz. Overall, D-tests suggested an increase in power output as a result of MFC operation in R-PWM mode. To elaborate on this observation, MFC-1 and MFC-2 were operated for 3–5 days in the R-PWM mode with 95% duty cycle and external resistance values chosen based on R_{int} estimations obtained in the polarization tests. Then the operating mode was changed to constant connection and the MFCs were operated for another 3–5 days. To ensure optimal performance during this period, R_{ext} value was optimized in real time using the P/O algorithm described in the Section 2. This sequence of testing was repeated several times. Power outputs obtained during each MFC operation by the P/O algorithm, were used as a basis for comparison (control) with the R-PWM mode of operation, i.e., the R-PWM mode was compared with the highest attainable MFC power output. The results of this comparison are summarized in Table 1 (current and power outputs were estimated based on the last 24 h of operation). Interestingly, similar currents (and therefore similar Coulombic efficiencies) were observed, while both in MFC-1 and MFC-2 voltages and power outputs were consistently higher during R-PWM tests. Since at an influent acetate concentration of 900 mg L^{-1} the anodic liquid measurements showed acetate-limiting conditions with acetate levels below 40 mg L^{-1}, the tests were repeated where the influent concentration of acetate was doubled (1800 mg L^{-1}). The increased acetate load led to higher acetate concentrations in the anodic liquid (600–700 mg L^{-1}) and somewhat lower Coulombic efficiency. Nevertheless, the results given in Table 1 once again confirmed improved power output during R-PWM operation.

Overall, power outputs observed during R-PWM tests were in a range of 3.6–3.8 mW corresponding to a volumetric power density of 72–76 mW L^{-1}. This power density is not only higher than that observed during MFC operation using the P/O algorithm (2.6–4.5 mW or 51–70 mW L^{-1}, Table 1), but also is higher in comparison to the recently reported performance of a continuously operated MFC with a power density of 30–50 mW L^{-1} (Ahn and Logan, 2012).

Interestingly, the periodic and pulse modes of operation of catalytic reactors were observed to lead to an increased catalyst activity and therefore an increased volumetric performance (Silveston et al., 1995). Several mechanisms were proposed to explain the increased catalyst activity, including a change in the catalyst state in response to reactant concentration, a higher catalyst activity due to a transient state, and non-linear reaction kinetics (Roopsingh and Chidambaram, 1999; Silveston et al., 1995). While a direct comparison between the periodic operation of chemical reactors and the R-PWM mode of MFC operation might not be always justified, both systems feature catalysts with non-linear reaction kinetics. It can be suggested that at high-frequencies the R-PWM mode of MFC operation leads to a reduced activation and/or concentration losses due to changes in the biocatalytic activity. These losses are represented as R_2 in the equivalent circuit model (Fig. 4). Considering poor mixing within the carbon felt anode, carbon source (acetate) transport through the porous anode might be one of the important limiting factors, i.e., acetate concentration within the anode is expected to be significantly lower than its concentration in the bulk anodic liquid during MFC operation in the continuous mode (R_{ext} is constant). Importantly, R_{ext} disconnection during t_{off} part of each duty cycle (Eq. (1)) in the R-PWM mode of operation might terminate acetate consumption by anodophilic bacteria. Consequently, acetate concentration within the anode could be hypothesized to be increasing during t_{off} part of each cycle. As the cycle continues and R_{ext} is re-connected, the metabolism of anodophilic bacteria resumes, presumably at a higher acetate concentration. Several

Please cite this article in press as: Coronado, J., et al. Pulse-width modulated external resistance increases the microbial fuel cell power output. Bioresour. Technol. (2013), http://dx.doi.org/10.1016/j.biortech.2013.08.005

previous studies demonstrated a strong link between carbon source availability and MFC performance, including the effect of carbon source on R_{int} values (Martin et al., 2010; Pinto et al., 2011a). As metabolic activity of the anodophilic microorganisms resumes upon R_{ext} reconnection, the improved acetate availability is hypothesized to positively affect MFC performance. Indeed, the anodophilic microorganisms were shown to exhibit a non-linear (Monod or Haldane-like) kinetics of carbon source consumption with lower internal resistances observed at carbon source–non-limiting conditions (Hamelers et al., 2011; Manohar and Mansfeld, 2009; Marcus et al., 2007; Pinto et al., 2010). These hypotheses might require extensive validation using experimental methods such as electrode potential monitoring and EIS measurements (Martin et al., 2013) followed by a thorough model-based analysis.

4. Conclusion

R-PWM mode of MFC operation increased the average output voltage and the power output at operating frequencies above 100 Hz. By comparing power outputs of MFCs operated in the R-PWM mode and with a constant resistance equal to the estimated total internal resistance value, the R-PWM mode operation was demonstrated to improve MFC performance by up to 22–43%. Analysis of the output voltage profiles acquired during R-PWM tests showed the presence of slow and fast dynamic components. This process dynamics was successfully simulated by a simple equivalent circuit model suitable for real-time MFC control and performance optimization.

Acknowledgement

This research was partially funded by the Natural Sciences and Engineering Research Council of Canada (NSERC).

Appendix A. Equivalent circuit model

The equivalent circuit model consisted of two internal resistors (R_1 and R_2) and one internal capacitor (C) as shown in Fig. 4. The following first order differential equation describes voltage dynamics at the capacitor:

$$\frac{\partial U_c(t)}{\partial t} = \frac{U_{oc}}{C(R_1 + R_{ext})} - \frac{R_1 + R_2 + R_{ext}}{R_2 C(R_1 + R_{ext})} U_c(t) \quad (A1)$$

where $U_c(t)$ is the voltage at the internal capacitor, R_{ext} is the external resistance, U_{oc} is the apparent open circuit voltage.

By applying Kirchhoff's circuit law to the diagram in Fig. 4, the following analytical solution can be used to obtain MFC output voltage (U_{MFC}) as a function of time at low operating frequencies:

$$U_{MFC}(t) = (U_{oc} - U_c(t)) \frac{R_{ext}}{(R_1 + R_{ext})} \quad (A2)$$

where,

$$U_c(t) = U_{final} + (U_c|t_0 - U_{final}) e^{\frac{-t}{\tau}} \quad (A3)$$

Here, the capacitance final voltage U_{final} and the time constant τ are defined as:

$$U_{final} = U_{oc} \frac{R_2}{R_1 + R_2 + R_{ext}}, \tau = \frac{R_2(R_1 + R_{ext})}{(R_1 + R_2 + R_{ext})} C \quad (A4)$$

At high frequencies of R_{ext} connection/disconnection, the voltage over the capacitance is considered to be a constant equal to the value of U_{final}.

References

Ahn, Y., Logan, B., 2012. A multi-electrode continuous flow microbial fuel cell with separator electrode assembly design. Appl. Microbiol. Biotechnol. 93, 2241–2248.

Durr, M., Cruden, A., Gair, S., McDonald, J.R., 2006. Dynamic model of a lead acid battery for use in a domestic fuell cell system. J. Power Sources 161, 1400–1411.

Grondin, F., Perrier, M., Tartakovsky, B., 2012. Microbial fuel cell operation with intermittent connection of the electrical load. J. Power Sources 208, 18–23.

Hamelers, H.V.M., Ter Heijne, A., Stein, N., Rozendal, R.A., Buisman, C.J., 2011. Butler–Volmer–Monod model for describing bio-anode polarization curves. Bioresour. Technol. 102, 381–387.

Logan, B., 2010. Scaling up microbial fuel cells and other bioelectrochemical systems. Appl. Microbiol. Biotechnol. 85, 1665–1671.

Manohar, A.K., Mansfeld, F., 2009. The internal resistance of a microbial fuel cell and its dependence on cell design and operating conditions. Electrochim. Acta. 54, 1664–1670.

Marcus, A.K., Torres, C.I., Rittmann, B.E., 2007. Conduction-based modeling of the biofilm anode of a microbial fuel cell. Biotechnol. Bioeng. 98, 1171–1182.

Martin, E., Savadogo, O., Guiot, S.R., Tartakovsky, B., 2010. The influence of operational conditions on the performance of a microbial fuel cell seeded with mesophilic sludge. Biochem. Eng. J. 51, 132–139.

Martin, E., Savadogo, O., Guiot, S.R., Tartakovsky, B., 2013. Electrochemical characterization of anodic biofilm development in a microbial fuel cell. Appl. Electrochem. 43, 533–540.

Oh, S.-E., Logan, B.E., 2007. Voltage reversal during microbial fuel cell stack operation. J. Power Sources 167, 11–17.

Park, J.-D., Ren, Z., 2012a. High efficiency energy harvesting from microbial fuel cells using a synchronous boost converter. J Power Sources 208, 322–327.

Park, J.-D., Ren, Z., 2012b. Hysteresis controller based maximum power point tracking energy harvesting system for microbial fuel cells. J. Power Sources 205, 151–156.

Pinto, R.P., Srinivasan, B., Guiot, S.R., Tartakovsky, B., 2011. The effect of real-time external resistance optimization on microbial fuel cell performance. Wat. Res. 45, 1571–1578.

Pinto, R.P., Srinivasan, B., Manuel, M.-F., Tartakovsky, B., 2010. A two-population bio-electrochemical model of a microbial fuel cell. Bioresour. Technol. 101, 5256–5265.

Pinto, R.P., Srinivasan, B., Tartakovsky, B., 2011b. A unified model for electricity and hydrogen production in microbial electrochemical cells. In: 18th IFAC Word Congress, Milano, Italy.

Premier, G.C., Kim, J.R., Michie, I., Dinsdale, R.M., Guwy, A.J., 2011. Automatic control of load increases power and efficiency in a microbial fuel cell. J. Power Sources 196, 2013–2019.

Randles, J.E.B., 1947. Kinetics of rapid electrode reactions. Disc. Faraday Soc. 1, 11–19.

Roopsingh, G., Chidambaram, M., 1999. Periodic operation of bioreactors for autocatalytic reactions with Michaelis–Menten kinetics. Bioprocess Eng. 20, 279–282.

Saito, T., Mehanna, M., Wang, X., Cusick, R.D., Feng, Y., Hickner, M.A., 2011. Effect of nitrogen addition on the performance of microbial fuel cell anodes. Bioresour. Technol. 102, 395–398.

Silveston, P., Hudgins, R.R., Renken, A., 1995. Periodic operation of catalytic reactors – introduction and overview. Catalysis Today 25, 91–112.

Song, Y.-C., Yoo, K.S., Lee, S.K., 2010. Surface floating, air cathode, microbial fuel cell with horizontal flow for continuous power production from wastewater. J. Power Sources 195, 6478–6482.

Tender, L.M., Gray, S.A., Groveman, E., Lowy, D.A., Kauffma, P., Melhado, J., Tyce, R.C., Flynn, D., Petrecca, R., Dobarro, J., 2008. The first demonstration of a microbial fuel cell as a viable power supply: Powering a meteorological buoy. J. Power Sources 179, 571–575.

Woodward, L., Perrier, M., Srinivasan, B., Pinto, R.P., Tartakovsky, B., 2010. Comparison of real-time methods for maximizing power output in microbial fuel cells. AIChE J. 56, 2742–2750.

Woodward, L., Tartakovsky, B., Perrier, M., Srinivasan, B., 2009. Maximizing power production in a stack of microbial fuel cells using multiunit optimization method. Biotechnol. Prog. 25 (3), 676–682.

Wu, P.K., Biffinger, J.C., Fitzgerald, L.A., Ringeisen, B.R., 2012. A low power DC/DC booster circuit designed for microbial fuel cells. Process Biochem. 47, 1620–1626.

Yang, F., Zhang, D., Shimotori, T., Wang, K.-C., Huang, Y., 2012. Study of transformer-based power management system and its performance optimization for microbial fuel cells. J. Power Sources 205, 86–92.

Please cite this article in press as: Coronado, J., et al. Pulse-width modulated external resistance increases the microbial fuel cell power output. Bioresour. Technol. (2013), http://dx.doi.org/10.1016/j.biortech.2013.08.005